AN ALN PIEZOELECTRIC MICROACTUATOR ARRAY

D. Ruffieux, M.A. Dubois * and N.F. de Rooij **
Bio-Inspired Systems, Centre Suisse d'Electronique et de Microtechnique, Neuchâtel, Switzerland
*Laboratory of Ceramics, Swiss Federal Institute of Technology Lausanne, Switzerland
**Institute of Microtechnology, University of Neuchâtel, Neuchâtel, Switzerland
e-mail: david.ruffieux@csem.ch

ABSTRACT

This paper presents the design, fabrication and characterisation of a piezoelectric microactuator array, the key component of a remotely controlled, wireless, solar powered microsystem which should be capable of locomotion. The walking principle mimics the elliptical leg motion of walking animals by using a combination of multiple DOF surface micromachined piezoelectric actuators associated with wafer-through etched features that transmit and amplify the piezo-induced motion to the backside of the wafer. Aluminium nitride has been chosen as the thin film piezoelectric material since it is highly insulating and can be deposited repeatedly with very high quality. The characterisation of the fabricated structure shows very promising results in view of meeting the wireless locomotion challenge.

INTRODUCTION

In recent years, there has been a considerable research effort focused towards the realisation of microrobotic components or systems. As opposed to miniaturising existing devices, a more innovative and interesting approach, which better takes advantage of the lithographic fabrication limitations and advantages, is based on microactuator arrays where the cooperative work of many coordinated simple actuators generates interactions with the macro world. This concept, proposed by H. Fujita in the early 90's [1] has spawn lots of realisations, which led to the demonstration of several micro-conveying systems based on different actuation principles [2,3,4,5]. The realisation of a moving microrobot was however hindered by the lack of sufficiently protruding structures since both electrical and mechanical interfaces where located on the same side of the substrate, thus preventing the simple flipping of a conveyor. This problem has been solved in [6], where long silicon plates are rotated way out of the substrate by curing a V-groove polyimide joint, which can later be thermally actuated. The demonstrated walking microrobot is evidently tethered to power, since it consumes about one watt of power.

While following the same collective approach, our group attempts to fabricate a miniature wireless walking system, powered by a high voltage solar cell and whose direction and speed can be remotely controlled through an interface ASIC described in [7]. The system key component is the electromechanical transducer. A thermomechanical version reported in [8] has been realised to verify some concepts. As the next step towards the autonomous system, the new transducer that is presented here, is based on the combination of wafer-through deep reactive ion etching (DRIE) with piezoelectric thin film actuation. This combination is offering new opportunities for actuators or arrays, such as the possibility of having simple multiple DOF, high speed, high stroke, low power actuators that can generate more complex motions with conveniently separated interfaces that allow multiple chip module assembly.

ACTUATOR DESCRIPTION

Actuator structure

Figure 1 shows the structure of a single actuator, which is made of a wafer-through etched, long and narrow silicon cylinder connected via a central plate and torsional hinges to three piezoelectric bimorph beams that can be actuated independently. The resulting structure has 3-DOF and the leg tip can reach any position within an ellipsoid. The unique advantages of this structure are the separation of the mechanical and electrical interfaces on opposite wafer sides and the high lateral motion amplitude that can be achieved through the levering effect of the leg combined with significant vertical amplitude. The side of the actuator is about 400µm, a leg is 300µm high and 30µm wide.

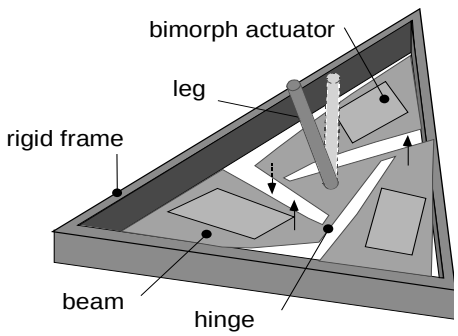

Figure 1: Structure of a single actuator

The elliptical motion can be generated through proper phasing of the three bimorphs. If the excitatory signals are all in phase, the plate and leg will move vertically. If one signal is inverted, the leg tip will start swinging horizontally. Signals in quadrature will produce the correct elliptical motion, either forth or back, in the selected direction. The two additional advantages that are gained by choosing this walking principle and a 3-DOF structure are the possible operation at mechanical resonance frequency resulting in a better energy coupling and the use of the same actuator for moving in any direction, thus improving the lifting and moving capability.

Arrayed configuration

A few hundreds of these walking cells are arranged into a hexagonal array, inside a triangular grid frame that provides stiffness and room for interconnection. The simplest gait, depicted in Figure 2, requires two phases so that half the actuators are in contact with the ground, where friction transmits their motion to the device, while the other half is preparing for the next step. Figure 3 shows the resulting actuators interconnections leading to six independent groups of beams.

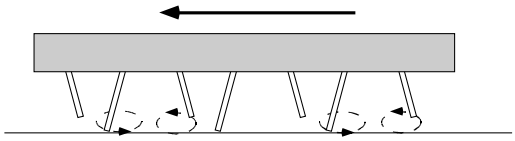

Figure 2: Walking principle

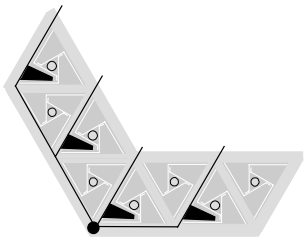

Figure 3: Schematic of the interconnections

DESIGN CONSIDERATIONS

Aluminium nitride for low frequencies applications

Aluminium nitride has not yet been applied widely for MEMS devices, since up to now ZnO or PZT thin films were being preferred apparently for processing reasons! Despite its somewhat lower coupling coefficient, aluminium nitride offers a great number of advantages over these two competing materials [9]. One is its excellent insulating properties, which makes it easy to use at low frequencies simply sandwiched between two conducting electrodes. A second is its low deposition temperature (400°C) and excellent chemical stability that makes it the piezoelectric material of choice for IC post-processing. Additionally, due to its high breakdown field (>800kV/cm) and since it is a non ferroelectric material thus requiring no poling, large field modulations and thus deflections are possible.

Deflection of the beam

Although the actuator is made of coupled beams, in the following design sections, we assume ideal hinges so that the beams essentially govern the actuator behaviour. The piezoelectric beam made of aluminium nitride is composed of four layers, a structural one, a bottom electrode, the piezoelectric thin film and the top electrode. After the last fabrication step, the legs are pushed away from the substrate by the resulting bending moment present in the beam. With σi, the residual stress and *ci*, the Young modulus of material *i*, the resulting bending moment yields

$$Mb = \sum_i w_i \cdot t_i \cdot \sigma_i \cdot (d_i - ym) \qquad (1)$$

where *wi, ti, di* are the width, thickness and distance to the beam edge from the middle of layer *i* and *ym* is the neutral axis given by

$$ym = \frac{\sum_i d_i \cdot t_i \cdot c_i}{\sum_i t_i \cdot c_i}. \qquad (2)$$

The moment induced by an electric field *Eel* applied across the thin film piezoelectric material can be written

$$Mp = w_p \cdot t_p \cdot e_{31} \cdot Eel \cdot (d_p - ym), \qquad (3)$$

where *e31* is the piezoelectric coefficient and is 1C/m² for a good qualiy AlN thin film. The resulting deflection at the tip of a beam of length *L* as a function of both internal and piezoelectrically induced stress is

$$y = \frac{(Mb + Mp) \cdot L^2}{2 \cdot EI} \qquad (4)$$

with *EI* the equivalent stiffness of the composite beam

$$EI = \sum_i c_i \cdot w_i \cdot \left[\frac{t_i^3}{12} + t_i \cdot (d_i - ym)^2 \right]. \qquad (5)$$

At that point, it is interesting to note that the deflection does not depend on the width of the beam, but on the square of its length and if all layers are scaled, the inverse of its thickness.

Energy coupling

The bending mechanical energy stored in the deformed beam due to the piezoelectric effect can be written

$$Wb = \frac{1}{2} \cdot \frac{Mp^2 \cdot L}{EI}, \qquad (6)$$

while the electrical energy is approximately the one stored in the dielectric capacitance of the film and is

$$Wel = \frac{1}{2} \cdot w_p \cdot t_p \cdot L \cdot \varepsilon_{33} \cdot \varepsilon_0 \cdot Eel^2 . \qquad (7)$$

The ratio of the two latter equations gives the bending electromechanical conversion efficiency

$$\eta = \frac{e_{31}^2}{\varepsilon_{33} \cdot \varepsilon_0 \cdot c_p} \cdot \frac{w_p \cdot t_p \cdot (d_p - ym)^2}{\sum_i \frac{c_i}{c_p} \cdot w_i \cdot \left[\frac{t_i^3}{12} + t_i \cdot (d_i - ym)^2 \right]} \qquad (8)$$

where the first term is the coupling coefficient k^2 of the piezoelectric material and the second a factor taking into account the structure of the composite beam that can be maximised for optimum bending efficiency.
At mechanical resonance, the amplitudes of motion are multiplied by the Q factor of the resonator and thus the bending energy by its square. In that case, the coupling efficiency, which is in the percent range in (8) increases considerably, even with low Q values.

Effect of beam shape

In order to find the most appropriate beam shape for the actuator, it is worth investigating what are the external loads against which the actuator will have to work and what are their effects on the beams. Figure 4 illustrates this for an ideal two-dimensional structure with two beams clamped on one side and connected with a pivot joint to a very rigid central plate and leg. The weight of the system, including an eventual payload will produce a gravity force, whose corresponding reaction force exerted by the ground will be shared among each leg. In that case, it is obvious that the beams bend so as to balance this load. Upon piezoelectric activation, the beams will act against this load and cancel some of this deflection while performing external work. On the other hand, lateral friction forces are generated at the leg ground interface during a horizontal displacement. These forces are counteracted by the activation of the piezoelectric beam in opposite directions. The friction forces turn into a bending moment in the bimorph plane, which is balanced by opposite reaction forces of the two beams.

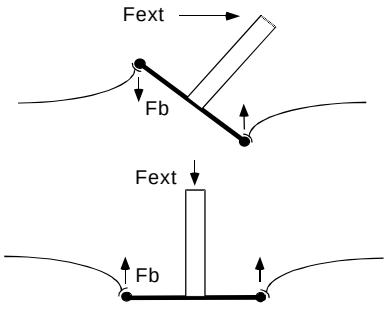

Figure 4: Illustration showing the loads applied to the actuator and the beams reaction.

The beams of the microactuator array will thus mostly act against forces only. It has been shown in [10] that the best shape for such a piezoelectric beam is triangular. By comparing a beam of constant width with a triangular one of same length and same surface (thus twice as large at its base) it is easy to show with the above formulas that the force which cancels the piezoelectric induced displacement –identical in both cases- is 33% greater for the tapered beam. This gain in energy is a consequence of the adequation between excitation and loading curves which are both quadratic in the latter case, while the deformation of a constant width beam due to an external force is of order three.

Scaling effects

The effects of the absolute geometrical dimension are now discussed based on the above equations. Scaling up the thickness of all the layers forming the bimorph results in a linear increase of the bending energy. Since the beam tip deflection is inversely proportional to this scaling factor, the force that can be exerted on the bimorph to compensate the piezo-induced deflection increases quadratically. Beside the technological factors limiting the thickness of the composite beam, the voltage and the energy that should be applied to generate the same electric field increase, becoming problematic in a wireless application, since the voltage has to be generated and switched onboard and the energy is limited.
Scaling down the two lateral dimensions of the beams results in a quadratic bending energy decrease, which is also affecting the beam deflection in the same way, meaning that the force remains constant. Now consider a given area and a fixed thickness so that the overall bending energy remains constant. Lateral downscaling means that the number of beams occupying this area increases quadratically. The overall force that compensates for the piezo-induced deflection follows the same increase rate, while the deflection decreases accordingly. There is thus a quadratic adaptation between force and deflection as the lateral dimensions are scaled. However, the resonance frequency of one such beam is inversely proportional to the square of its length, leading to a constant frequency deflection product, directly responsible for the leg tip speed. In that case, the consumed power increases accordingly, but both high-force and high-speed devices can be achieved simultaneously.

FABRICATION

Process flow

The fabrication of the piezoelectric actuator array uses a combination of surface and bulk micromachining. Figure 5 shows a cross-section of the five-mask fabrication process.

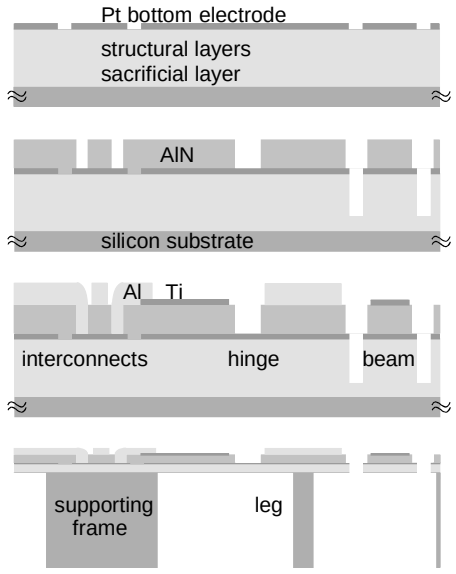

Figure 5: Cross-section illustrating process flow

On a 300µm thick, double sides polished wafer a sacrificial/etch-stop CVD oxide and a structural layer made of polysilicon and a low stress nitride are deposited. The bottom electrode made of a <111> oriented platinum layer required for subsequent high quality piezoelectric thin film growth is then deposited and dry etched to define the actuator structure and the interconnects. A high quality c-axis oriented AlN layer is then sputter deposited at 400°C and patterned in hot phosphoric acid to free the beam edges, hinges and to open contacts on top of the earlier defined platinum strips. The structural material is then dry etched before the titanium or titanium/platinum top electrode is deposited and patterned. A thick aluminium layer is evaporated and patterned to bring electrical signals to the actuators and stiffen the central plate holding the leg. A backside thick resist photolithography is then performed before the wafer is DRIE etched through until the etch-stop oxide is reached. This sacrificial layer and the protective topside resist are then removed in buffered HF and acetone, releasing the structures that bend down due to the stress distribution across the bimorph.

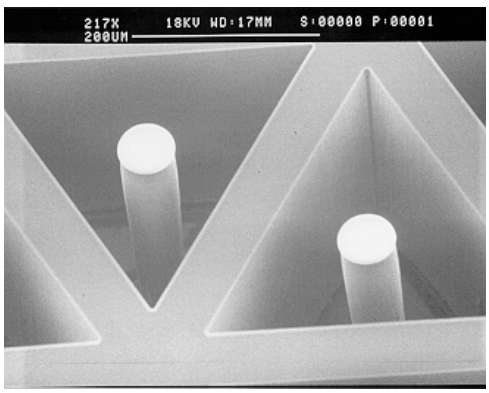

Figure 6: SEM view of two wafer-through etched legs

Figure 6 shows a SEM picture of two fabricated legs and Figure 7 an optical micrograph showing a view of a few actuators

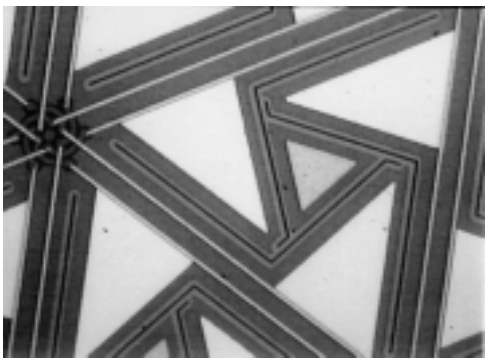

Figure 7: Optical micrograph showing an actuator

Stress control

A relatively precise stress control of all the layers forming the composite beam is essential to ensure that it bends downwards in a controllable fashion upon releasing, thus pushing the legs away from the substrate. Additionally, a tensile etch stop layer is also desired to maintain the membrane flat once the bulk silicon has been completely removed under the actuators and avoid their breakage due to membrane buckling. The etch-stop material of choice for wafer-through cryogenic DRIE is thermal oxide, since it serves simultaneously as a masking material for the DRIE on the opposite wafer side due to its very low etch rat compared to silicon. With ambient DRIE process, this selectivity drops considerably, meaning that thick resist masks are preferred to make wafer-through etching. It also leads to an increase of the etch-stop layer thickness, especially if overetching is necessary to compensate for the radial etch rate inhomogeneity. Since thermal oxide is quite heavily compressive, it can be advantageously replaced by CVD oxide, which remains slightly tensile (about +100MPa) if it is not annealed above 700°C. Considering the bimorph again, and neglecting the electrodes effect, one can feel that the structural material has to be tensile and the piezoelectric material compressive for the beams to effectively bend down upon release. While most thin film piezoelectric material naturally exhibit compressive stress, it is much harder to obtain a low stress or slightly tensile structural material. Doped polysilicon can be made slightly compressive (around –30MPa) but at an anneal temperature of 1025°C which would restore a highly compressive stress in the CVD oxide. Low stress nitride is a good candidate, but it suffers from a low deposition rate and low throughput. On the other hand, as demonstrated in [11], polysilicon deposited in a semi-amorphous phase at 570°C can exhibit a somewhat highly tensile residual stress upon annealing at 600°C. In this work, a combination of these two materials has been chosen for the structural material of the composite

beam. The deposition and annealing of the semi-amorphous polysilicon, which forms most of the structural layer, is followed by this of an insulating PECVD nitride layer, whose stress can be adjusted to compensate the run to run variations of the polysilicon one. The stress of the bottom platinum electrode is not of concern, since this layer is located very close to the neutral axis of the bimorph. The case of the upper electrode is very different if it is made of a very tensile material, such as evaporated platinum that exhibits a tensile residual stress in the GPa range. When combined with a location far away from the neutral axis, this thin layer introduces a considerable bending moment and its thickness can thus be varied so as to provide a considerable tuning effect on the beam final deflection. Aluminium nitride can be deposited with a broad stress range either in a tensile or compressive state. However the later seems to favour its piezoelectric activity. For this application a stress in the vicinity of -200MPa was at aim.

Deep reactive ion etching

Considerable developments on DRIE process were carried out in both cryogenic and ambient systems. The most important parameter, when etching wafer-through, high aspect ratio structures such as the legs, is the lateral etch rate homogeneity of the system. The typical 10-15% inhomogeneity of the first generation of ambient etchers yields tremendous problems in getting standing legs. Once the etch stop layer is reached, the etching dynamics greatly changes, quickly leading to leg slashing if the structures are overetched. Increasing the passivation in that case, somewhat allows for opened structures to be preserved while adjacent ones are being opened but the reduced etch rate increases processing time significantly. On a cryogenic system, the passivation can be increased while maintaining significant etch rate and obtaining groups of standing legs was easier. Cryogenic and ambient second generation etchers achieve a much better radial homogeneity hopefully eliminating this problem.

MEASUREMENTS

At that time, only individual test actuators and beams have been measured due to the presence of frequent pinholes in the AlN, inevitably leading to shorted devices in the arrayed configuration. Resist residues left on top of the platinum after ion milling are believed to react with nitrogen during AlN deposition and be responsible for the shorts since many hillocks twice as high as the AlN itself could be seen with the SEM afterwards. The following measurements are somewhat lacking coherence since not so much material was available thus far due to yield problems thus preventing direct comparison between graphs. They give nevertheless an overview of the possible measurements that can be made to characterise the 3-DOF structure.

Measuring setup

In order to characterise individual actuators, the following setups have been used. The impedance of individual beams has been measured with an HP4194A so as to extract some resonator's properties. The vertical mechanical frequency response of test actuators has been obtained interferometrically, while a confocal microscope has yielded the quasi-static response. The tilting behaviour has been obtained with the setup shown in Figure 8, where a focused laser beam is reflected by the tilted actuator and the resulting lateral beam shift is analysed with a four quadrants or lateral photodiode. Simple geometrical calculations then lead to the leg trajectory.

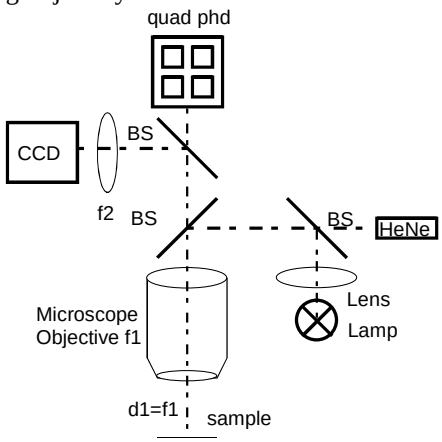

Figure 8: Measuring setup for tilting motion

Electrical impedance measurement

Figure 9 shows the measured electrical impedance of a beam near its first resonance frequency. Curve fitting yields a Q-factor of 110, a motional over static capacitance ratio of 0.1% and a tanδ of 1.7% at 25kHz.

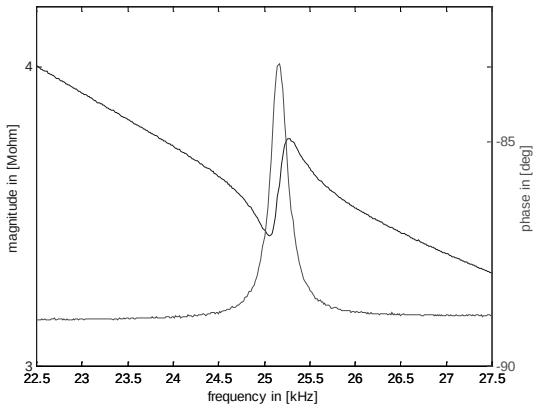

Figure 9: Impedance measurement of a single beam

Quasi-static response

Figure 10 shows the quasi-static response of the same beam when the electric field is varied linearly between

±200kV/cm or ±10V together with the theoretical value (4). The breakdown field was close to 800kV/cm.

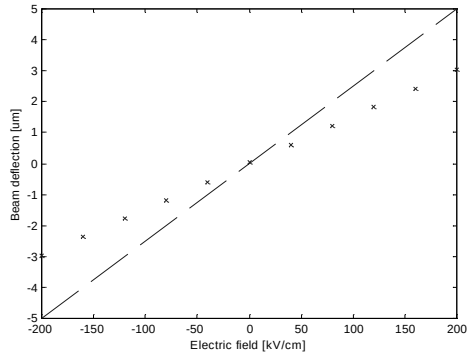

Figure 10: Beam displacement versus electric field (dashed line: theoretical, dots: measured values)

Quasi-static elliptical motion

The quasi-static extreme positions that the leg reaches during the elliptical motion are shown in Figure 11. The vertical amplitude was obtained with the confocal microscope while the lateral one with the tilting setup described earlier when the actuators were connected to either +10V or –10V as it is planned in the system.

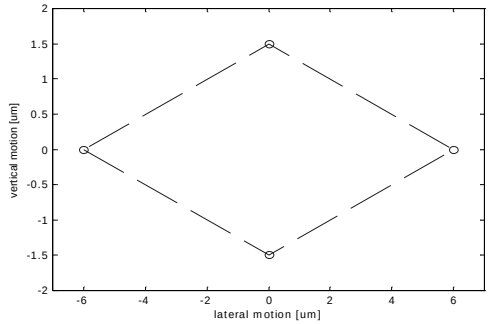

Figure 11: Quasi-static tip of the leg trajectory

Interferometric measurements

Figure 12 shows an interferometric measurement of the vertical frequency response of an actuator where a Q of 14 can be extracted for the main resonance at 33kHz.

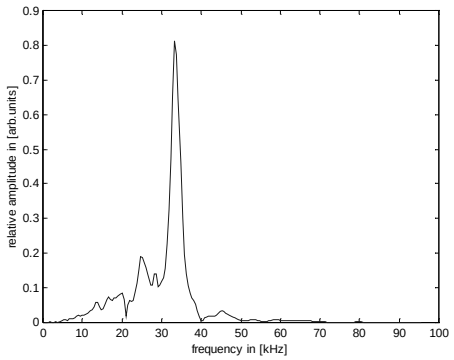

Figure 12: Vertical frequency response of an actuator

CONCLUSIONS

The fabrication of a low-power aluminium nitride piezoelectric microactuator array designed as part of a batch fabricated wireless locomotion system has been demonstrated. The measurements performed so far on test actuators have shown the possibility of generating lateral amplitudes of motion exceeding 10µm and vertical ones in the range of 3µm in quasi-static operation. At mechanical resonance, these amplitudes are likely to be multiplied by the Q factor of the resonator, which was about 14 for the vertical mode. A better cleaning procedure after the bottom electrode ion milling is essential to take full advantage of the excellent aluminium nitride thin film properties that were demonstrated in earlier work, since unstable resist residues lead to many shorts between the top and bottom electrodes and degraded the film electrical properties. Getting high yield, stress optimised structures is now of primary interest for the in depth characterisation of the different designs before the assembly of the system is addressed.

ACKNOWLEDGEMENTS

The authors are grateful to J. Baborobsky and P.A. Clerc for their help in ion milling and DRIE.

REFERENCES

[1] H. Fujita, K. Gabriel, “New opportunities for Micro Actuators”, Proc. Int. Conf. on Solid-State Sensors and Actuators, June 1991, pp. 14-20.

[2] M. Ataka, A. Omodaka, N. Takeshima, H. Fujita, “Fabrication and Operation of Polyimide Bimorph Actuators for a Ciliary Motion System”, JMEMS, Vol 2, No 4, Dec 1993, pp 147-150.

[3] K.F. Bohringer, B.R. Donald, N.C. MacDonald, “Single-Crystal Silicon Actuator Arrays for Micro Manipulation Tasks”, Proc. MEMS 1996, June 1996, pp. 7-12.

[4] J.F.L. Goosen, R.F. Wolffenbuttel, “Object Positioning using a Surface Micromachined Distributed System”, Transducers 95, June 1995, pp. 396-399, Stockholm, Sweden

[5] C. Liu, T. Tsao, Y.C. Tai, W. Liu, P. Will, C.M. Ho, “A Micromachined Permalloy Magnetic Actuator Array for Micro Robotics Assembly Systems”, Transducers 95, June 1995, pp. 328-331, Stockholm, Sweden.

[6] T. Ebefors, J.U. Mattson, E. Kälvesten, G. Stemme, ”A Silicon Walking Microrobot”, Transducers 99, June 1999, on CD-ROM, Sendai, Japan.

[7] D. Ruffieux, “A Low Power ASIC for the Control of a Mobile Microactuator Array,” Proc. ESSCIRC 99, Sept. 1999, pp. 90-93, Duisburg, Germany.

[8] D. Ruffieux, N.F. de Rooij, “A 3-DOF Bimorph Actuator Array Capable of Locomotion”, Proc. EUROSENSORS XIII, Sept. 1999, on CD-ROM, The Hague, The Netherlands.

[9] M.A. Dubois. P. Muralt, “Properties of AlN Thin Films for Piezoelectric Transducers and Microwave Filter Applications”, App. Phys. Letters, Vol. 74, No. 20, May 1999, pp. 3032-3034.

[10] I. Lucas. “Transformation of Energy in Piezoelectric Drive Systems ”, Siemens Forsch.- u. Entwickl.-Ber. Bd. 4 (1975) Nr. 6, Springer-Verlag, pp. 373-379.

[11] P.J. French et al., “The Development of a Low-Stress Polysilicon Process Compatible with Standard Device Processing ”, JMEMS, Vol 5, No 3, Sept. 1996, pp. 187-196.